

# Prompt-based Distribution Alignment for Unsupervised Domain Adaptation

Shuanghao Bai<sup>1</sup>, Min Zhang<sup>2</sup>, Wanqi Zhou<sup>1,4</sup>, Siteng Huang<sup>2</sup>, Zhirong Luan<sup>3</sup>,  
Donglin Wang<sup>2\*</sup>, Badong Chen<sup>1\*</sup>

<sup>1</sup>Institute of Artificial Intelligence and Robotics, Xi'an Jiaotong University, Xi'an, China

<sup>2</sup>Westlake University Institute of Advanced Technology, Westlake Institute for Advanced Study

<sup>3</sup>School of Electrical Engineering, Xi'an University of Technology, Xi'an, China <sup>4</sup>RIKEN AIP

## Abstract

Recently, despite the unprecedented success of large pre-trained visual-language models (VLMs) on a wide range of downstream tasks, the real-world unsupervised domain adaptation (UDA) problem is still not well explored. Therefore, in this paper, we first experimentally demonstrate that the unsupervised-trained VLMs can significantly reduce the distribution discrepancy between source and target domains, thereby improving the performance of UDA. However, a major challenge for directly deploying such models on downstream UDA tasks is prompt engineering, which requires aligning the domain knowledge of source and target domains, since the performance of UDA is severely influenced by a good domain-invariant representation. We further propose a **Prompt-based Distribution Alignment (PDA)** method to incorporate the domain knowledge into prompt learning. Specifically, PDA employs a two-branch prompt-tuning paradigm, namely base branch and alignment branch. The base branch focuses on integrating class-related representation into prompts, ensuring discrimination among different classes. To further minimize domain discrepancy, for the alignment branch, we construct feature banks for both the source and target domains and propose image-guided feature tuning (IFT) to make the input attend to feature banks, which effectively integrates self-enhanced and cross-domain features into the model. In this way, these two branches can be mutually promoted to enhance the adaptation of VLMs for UDA. We conduct extensive experiments on three benchmarks to demonstrate that our proposed PDA achieves state-of-the-art performance. The code is available at <https://github.com/BaiShuanghao/Prompt-based-Distribution-Alignment>.

## 1 Introduction

Unsupervised domain adaptation (UDA) aims to improve the generalization performance in the target domain of the pre-trained model by using the labeled source domain and unlabeled target domain (Wilson and Cook 2020; Zhu et al. 2023a). Many methods have been proposed to address the UDA problem, mainly including adversarial training (Ganin and Lempitsky 2015; Rangwani et al. 2022) and metric learning (Saito et al. 2018; Tang, Chen, and Jia 2020; Zhang,

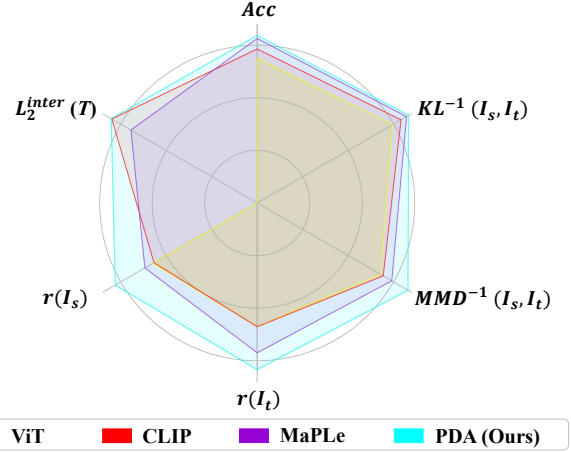


Figure 1: Metric comparisons on Office-Home. Higher values are better.  $r$  measures the compactness of features (*i.e.*, the division of inner-class  $L_2$  distance and inter-class  $L_2$  distance  $L_2^{inter}$ ). MMD and KL divergence measure the domain discrepancy.  $T$ ,  $I_s$  and  $I_t$  denote the text features, and image features of the source and target domain, respectively. Our method demonstrates the most discriminable text features, the most compact image features, the lowest domain discrepancy, and the best accuracy.

Wang, and Gai 2020). However, mitigating distribution by domain alignment may inadvertently result in a loss of semantic information, which comes from the entangled nature of semantic and domain information (Tang, Chen, and Jia 2020; Ge et al. 2022; Zhang, Huang, and Wang 2022).

Recently, large vision language models (VLMs) like CLIP (Radford et al. 2021) have shown impressive generalization performance in various downstream tasks. With the disentangled visual and semantic representations, this may avoid the loss of semantic information and improve UDA performance. In light of this, we conduct an empirical experiment to demonstrate the applicability of VLMs to the UDA problem. Specifically, we evaluated the performance of both unimodal model Vision Transformer (ViT) (Dosovitskiy et al. 2021) and zero-shot CLIP with hand-crafted prompts. In Figure 1, although the compactness of source features  $r(I_s)$  and target features  $r(I_t)$  of CLIP is similar to

\*Corresponding authors.

that of supervised-trained ViT, yet maximum mean discrepancy (MMD) and KL divergence (KL) minimize, resulting higher accuracy of target domain (Acc). This indicates CLIP has the potential to minimize the domain discrepancy for UDA, which benefits from the multi-modal interaction.

To further adapt VLMs to downstream UDA tasks, one of the most efficient paradigms is prompt tuning. Current state-of-the-art prompt tuning methods, such as CoOp (Zhou et al. 2022b) and MaPLe (Khattak et al. 2023), have demonstrated superior performance on some specific downstream tasks. CoOp method adopts soft prompts to learn an appropriate text prompt, and MaPLe further introduces vision-language prompts to ensure mutual synergy. As shown in Figure 1, we observe that 1) MaPLe takes a step towards aligning domains compared to CLIP, as evidenced by its lower KL divergence and MMD, which indicates that *the prompts tuning can help minimize the domain shift*. 2) The image features of MaPLe are more compact, indicating *prompt tuning can further improve the discriminative ability of CLIP model*. Nonetheless, these prompt tuning methods such as CoOp or MaPLe may not be sufficient to address the domain shift problem fully because these methods primarily focus on the placement of the prompt and may not directly tackle the underlying causes of the domain shift. Therefore, we argue that prompts should not only focus on their design but also adapt to different domains by incorporating domain knowledge into the prompt.

To this end, we propose a **Prompt-based Distribution Alignment (PDA)** method for UDA. PDA consists of two branches, namely the base branch and the alignment branch. The base branch generates the image and text representations with prompt tuning, which focuses on integrating class-related representations into prompts, ensuring discrimination among different classes for each domain. The principal objective for UDA is to minimize the distribution shift of image representations. The alignment branch utilizes image representations to introduce domain knowledge to minimize the domain discrepancy. To achieve this, we first construct a source-domain and target-domain feature bank and propose image-guided feature tuning (IFT) to make the image representations of inputs attend to feature banks, which can effectively integrate self-enhanced and cross-domain features into the model. As shown in Figure 1, PDA not only excels in obtaining more discriminable image and text representations but also effectively mitigates the domain discrepancy. Therefore, our method can guarantee the discriminability of the model, and effectively capture important features from both the source and target domains, which enables domain alignment and allows the model to better adapt to the target domain. Our main contributions are as follows:

- We first experimentally verify the effectiveness of VLM on UDA downstream tasks. Then, based on this finding, we further propose a prompt-based distribution alignment (PDA) method to tune prompt to the target domain.
- The proposed PDA includes two training branches. First, the base branch ensures discrimination among different classes. Second, the aligned branch obtains the domain-invariant information by image-guided feature tuning.

- Extensive experiments demonstrate the effectiveness of the proposed PDA, which achieves state-of-the-art performance on Office-Home, Office-31 and VisDA-2017.

## 2 Related Work

### 2.1 Unsupervised Domain Adaptation

Unsupervised domain adaptation (UDA) aims to align the source and target domains by learning a domain-invariant feature representation (Zhang et al. 2023b; Chen, Xiao, and Kuang 2022; Xiao et al. 2022). One method of aligning domains is minimizing divergence between different domains. Many divergence measures have been proposed, such as maximum mean discrepancy (MMD) (Long et al. 2015), correlation alignment (CORAL) (Sun, Feng, and Saenko 2016) and maximum density divergence (MDD) (Zhang et al. 2019). Another line of work is motivated by the success of adversarial learning. By modeling the optimization process as a minimax problem (Ganin and Lempitsky 2015; Long et al. 2018; Rangwani et al. 2022; Xiao et al. 2021), a domain discriminator is introduced to distinguish the samples from different domains, with the aim of training the model to generate domain-invariant features that can deceive the domain discriminator. With the advent of transformer models, TVT (Yang et al. 2023) proposes an adaptation module to obtain both transferable and discriminative features, and CDTrans (Xu et al. 2022) leverages the robustness of cross-attention modules and proposes a cross-domain transformer for direct feature alignment. Different from these mainstream unimodal UDA methods, we focus on harnessing the transferability inherent in vision language models, which exhibit a promising capacity for domain alignment due to multimodal interaction.

### 2.2 Vision Language Models

The pre-trained Vision Language Models (VLMs) learn image-text correlation by various pre-training tasks, such as masked language modeling (Kim, Son, and Kim 2021), masked language modeling (Tan and Bansal 2019), image-text matching (Huang et al. 2021) and contrastive learning (Jia et al. 2021; Zhang et al. 2022a; Chen et al. 2021). Although these models have achieved unprecedented success across a wide range of tasks including zero-shot and few-shot visual recognition, effectively adapting them to downstream tasks remains a formidable challenge. Many works have been proposed to enhance the generalization ability on downstream tasks by introducing additional feature adapter (Gao et al. 2021; Zhang et al. 2023a; Bai et al. 2024), attention (Guo et al. 2023), cache model (Zhang et al. 2022b) and so on. The prompt learning paradigm, initially employed in the field of Natural Language Processing (NLP), has also been integrated into VLMs, emerging as one of the most efficient approaches for fine-tuning VLMs on various downstream tasks. In this work, we follow the line of prompt learning methods and propose a prompt-based distribution alignment method to improve the transferability of CLIP for addressing the UDA problem.

### 2.3 Prompt Tuning in Vision Language Models

Prompt tuning is one of the important parts of parameter-efficient tuning, which aims at learning only a small number of parameters by means of input composition (Pfeiffer et al. 2023; Zhu et al. 2023b) while keeping the large model fixed. CoOp (Zhou et al. 2022b) firstly introduces soft prompt in VLMs, demonstrating that suitable text prompts can enhance image recognition performance. CoCoOp (Zhou et al. 2022a) extends the CoOp by integrating lightweight neural networks to dynamically generate prompts for individual images to deal with the overfitting problem of prompts. VPT (Jia et al. 2022) achieves impressive results using a few visual prompts in transformer models. Furthermore, MaPLe (Khattak et al. 2023) combines both text and visual prompts into CLIP to improve the alignment between text and image representations. To exploit the effectiveness of prompt tuning for UDA, we introduce a two-branch training paradigm consisting of base and alignment branches. The base branch leverages prompt tuning to enhance the discriminability of CLIP model. For the alignment branch, we design an image-guided feature tuning to mitigate domain discrepancy.

## 3 Preliminaries

### 3.1 Unsupervised Domain Adaptation

UDA focuses on improving the model’s generalization performance with the labeled data from the source domain and unlabeled data from the target domain. Formally, given a labeled dataset  $D_s = \{x_i^s, y_i^s\}_{i=1}^{n_s}$  of the source domain and unlabeled dataset  $D_t = \{x_j^t\}_{j=1}^{n_t}$ , where  $n_s$  and  $n_t$  denote the size of samples in the source and target domains, respectively. Note that the data of two domains are sampled from two different distributions, and we assume that the two domains share the same label space. We denote the input space as  $X$  and denote the label set as  $Y$ . There is a mapping  $M : \{X\} \rightarrow Y$  from images to labels. In this work, we incorporate prompts  $V$  into the input, thus the mapping could be rephrased as  $M : \{X, V\} \rightarrow Y$  from images and prompts to labels. Our goal is to mitigate the issue of domain discrepancy between  $D_s$  and  $D_t$ , and to learn a generalized prompt  $P$  that can facilitate the transfer of knowledge from the source domain to the target domain.

### 3.2 Revisiting Prompt Learning

Contrastive Language-Image Pre-Training (CLIP) model consists of an image encoder and a text encoder, which encodes images and corresponding natural language descriptions, respectively.

**Zero-shot inference.** The pre-trained CLIP model is adapted to downstream tasks with hand-crafted prompts, rather than fine-tuning the model. The text is always manually designed as ”a photo of a [CLASS]” ([CLASS] is the class token). The image-text matching score is computed using the cosine similarity  $sim(w_i, z)$  between the image representation  $z$  and the text representation  $w_i$  corresponding to the  $i$ -th class. The image representation is derived from the image encoder with an input image, while the text representation  $w_i$  is extracted from the text encoder using the prompt

description associated with the  $i$ -th class. The probability of the image belonging to the  $i$ -th class can be formulated as:

$$p(y = i | x) = \frac{\exp(sim(w_i, z) / t)}{\sum_{j=1}^K \exp(sim(w_j, z) / t)}, \quad (1)$$

where  $t$  denotes temperature parameter,  $K$  denotes the number of classes and  $sim$  denotes the cosine similarity.

**Text prompt tuning.** It avoids prompt engineering manually and strengthens the transferring ability of CLIP. CoOp (Zhou et al. 2022b) introduces a set of  $M$  continuous learnable context vectors  $v = [v^1, v^2, \dots, v^M]$ , then the  $i$ -th class of text prompt  $t^i$  is defined as  $t^i = [v, c^i]$ , where  $c^i$  is the fixed input token embedding. The learnable context vectors can be extended to deeper transformer layers of the text encoder with transformer-based architecture, thus each layer of input can be rephrased as  $[v_j, c_j]_{j=1}^J$ , where  $J$  is the number of transformer layers in the text encoder and  $[\cdot, \cdot]$  refers to the concatenation operation.

**Visual prompt tuning.** It adopts a similar paradigm as text prompt tuning, where additional context vectors that are fed into each layer of the image encoder are automatically learned. For transformer-based image encoder, VPT (Jia et al. 2022) inserts a collection of prompts  $\tilde{v}$  between a sequence of patch embeddings  $e$  and the learnable class token  $c$ , which can be designed as  $[\tilde{v}_j, e_j, c_j]_{j=1}^J$ .

**Multi-modal prompt tuning.** The text prompt  $v$  and visual prompt  $\tilde{v}$  are combined into CLIP. For instance, MaPLe (Khattak et al. 2023) tunes the vision and language branches of CLIP together by sharing prompts across both modalities.

## 4 Method

Inspired by the observations in the previous section, we attempt to design an efficient yet effective prompt tuning method for UDA. To enhance the transferability of the prompt, we propose a Prompt-based Distribution Alignment (PDA) method, whose framework is illustrated in Figure 2. We introduce our PDA method as follows.

### 4.1 Prompting for Base Branch

**Prompt design.** We mainly adopt the paradigm of multi-modal prompt. For the early layers of the image encoder, a text prompt is employed to generate a visual prompt by a projection layer. This means that text prompts are employed to guide the encoding process of images, enabling the images to possess information in the feature space that is relevant to the given text, therefore achieving alignment of images with pertinent textual information. For the later layers of the image encoder, each layer utilizes an independent prompt. This design allows each layer to independently capture distinct visual and semantic features of the image, enabling better image-text interaction and capturing different visual and semantic features.

**Loss function.** Contrastive loss function is then employed to align the image and text representations, which can be formulated as:

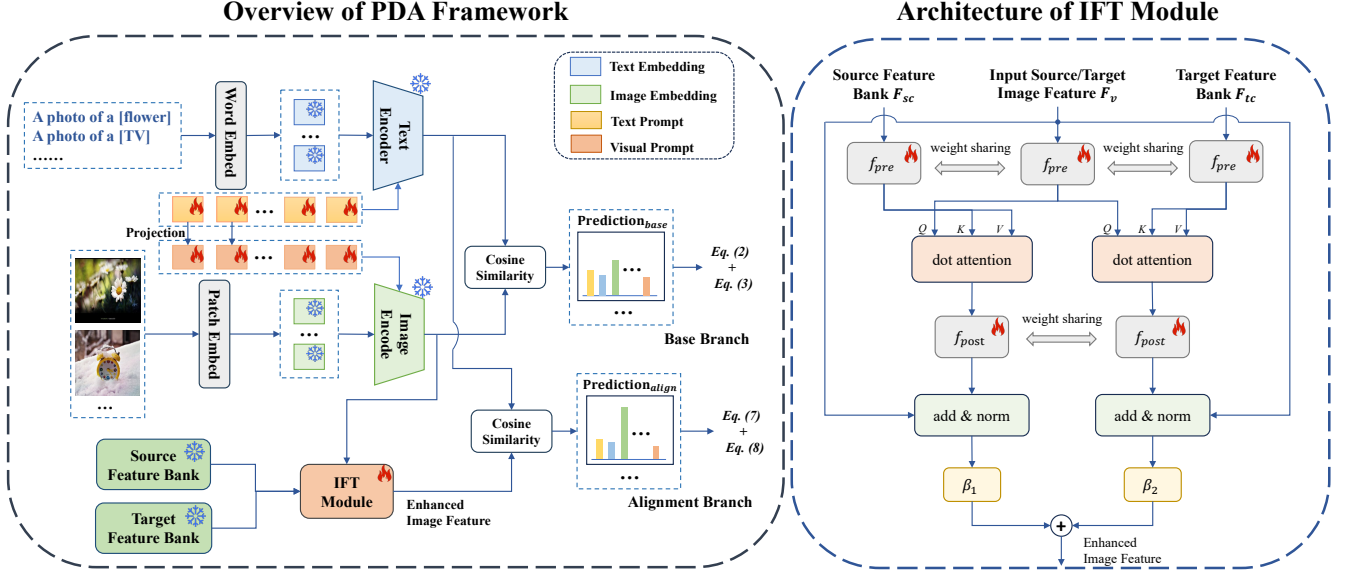


Figure 2: Overview of the proposed Prompt-based Distribution Alignment (PDA) method. The snow denotes the frozen parameters, and the fire denotes the learnable parameters. From left to right, we respectively show the detailed framework of PDA and the architecture of the IFT module. We mainly adopt the multi-modal prompt tuning in our PDA method. Additionally, IFT module makes the visual features attend to the source/target-domain feature bank for domain alignment.

$$\mathcal{L}_x = - \sum_i y_i^s \log \frac{\exp(\text{sim}(\hat{w}_i, \hat{z}^s)/t)}{\sum_{j=1}^K \exp(\text{sim}(\hat{w}_j, \hat{z}^s)/t)}, \quad (2)$$

where  $y^s$  denotes the one-hot ground-truth of source domain data,  $K$  is the number of classes,  $w_i$  and  $\hat{z}^s$  denote the  $i$ -th class of final text representation and final image representations of the source domain with prompt tuning, respectively.

To further exploit data of the target domain, we use pseudo labels to train these unlabeled data like Ge et al. (Ge et al. 2022). The pseudo labels are generated by the prediction of CLIP model. In order to enhance the reliability of these pseudo labels, we set a fixed threshold value  $\tau$ . If the maximum probability  $\tau_p$  predicted by CLIP for a given image is lower than this threshold, the pseudo label is discarded. Again, we adopt the contrastive loss function:

$$\mathcal{L}_u = -\mathbb{I}(\tau_p \geq \tau) \sum_i \hat{y}_i^t \log \frac{\exp(\text{sim}(\hat{w}_i, \hat{z}^t)/t)}{\sum_{j=1}^K \exp(\text{sim}(\hat{w}_j, \hat{z}^t)/t)}, \quad (3)$$

where  $\mathbb{I}(\cdot)$  is an indicator function,  $\hat{y}^t$  denotes the one-hot pseudo label of target domain data and  $\hat{z}^t$  denotes final image representations of the target domain with prompt tuning.

## 4.2 Pipeline of Alignment Branch

For the alignment branch, we construct feature banks for both the source and target domains and propose image-guided feature tuning (IFT) to make the input attend to feature banks to achieve domain alignment.

**Constructing feature banks.** With access to data from both the source and target domains, we can obtain text features

and image features from both domains. Based on the strong zero-shot ability of CLIP, we could construct robust and accurate feature banks. Firstly, we produce confidence scores (*i.e.*, maximum probability) for images in the source domain with the prediction in zero-shot CLIP. Similarly, we generate a confidence score and corresponding pseudo label for each image in the target domain. Specifically, the index of the maximum confidence score is the pseudo label of the image. We select the visual features of images with top- $C$  confidence scores in each class for the source and target domains, and construct a  $K$ -way  $C$ -shot source-domain feature bank and target-domain feature bank, where  $K$  denotes the number of classes and  $C$  denotes the number of samples in each class. Then we obtain the centroid features of each class as the final source-domain feature bank  $z_{sc}$  and target-domain feature bank  $z_{tc}$ , respectively.

**Image-guided feature tuning (IFT).** IFT leverages feature banks to guide images to obtain self-enhanced and cross-domain features, as shown in Figure 2 (right). We first apply a weight-shared projector layer  $f_{pre}$ , *i.e.*, a three-layer multilayer perceptron, to transform the image feature  $\hat{z}$ , source-domain feature bank  $z_{sc}$ , and target-domain feature bank  $z_{tc}$  into query, key and value, which can be formulated as:

$$Q = f_{pre}(\hat{z}), \quad K_{sc}, V_{sc} = f_{pre}(z_{sc}), \quad (4)$$

$$K_{tc}, V_{tc} = f_{pre}(z_{tc}).$$

We make the image feature attend to source-domain and target-domain feature banks, resulting in augmented image features. These features are then transformed by another weight-shared projector  $f_{post}$ . The whole process with attention can be formulated as:

Method	A-C	A-P	A-R	C-A	C-P	C-R	P-A	P-C	P-R	R-A	R-C	R-P	Avg
zero-shot CLIP	67.6	89.0	89.4	82.4	89.0	89.4	82.4	67.6	89.4	82.4	67.6	89.0	82.1
linear probe CLIP	60.1	73.7	80.9	66.4	76.4	76.8	63.4	61.0	82.3	74.7	64.8	88.3	72.4
CoOp	70.0	90.8	90.9	83.2	90.9	89.2	82.0	71.8	90.5	83.8	71.5	92.0	83.9
CoCoOp	70.4	91.4	90.4	83.5	91.8	90.3	83.4	70.9	91.0	83.4	71.2	91.7	84.1
VP	66.7	89.1	89.1	81.7	89.0	89.2	81.8	67.0	89.1	81.7	66.6	89.0	81.7
VPT-shallow	69.3	90.1	90.2	83.4	91.0	90.2	82.6	70.6	90.9	83.5	69.6	91.2	83.6
VPT-deep	71.6	89.9	90.3	82.8	91.0	89.7	82.0	71.5	90.3	84.6	71.7	91.6	83.9
IVLP	71.4	<b>91.7</b>	90.8	83.6	90.2	89.3	82.2	72.4	90.4	84.1	72.1	92.0	84.2
MaPLe	72.2	91.6	90.3	82.6	90.9	89.8	82.4	71.6	90.1	85.1	72.0	92.1	84.2
DAPL	70.7	91.0	90.9	85.2	91.0	91.0	85.1	70.7	90.9	85.3	70.4	91.4	84.4
<b>PDA (Ours)</b>	<b>73.5</b>	91.4	<b>91.3</b>	<b>86.0</b>	<b>91.6</b>	<b>91.5</b>	<b>86.0</b>	<b>73.5</b>	<b>91.7</b>	<b>86.4</b>	<b>73.0</b>	<b>92.4</b>	<b>85.7</b>

Table 1: Comparisons with the prompt tuning methods on Office-Home dataset with ViT-B/16 as the backbone. Bold denotes the best scores.

Method	A-D	A-W	D-A	D-W	W-A	W-D	Avg
zero-shot CLIP	77.7	75.8	79.0	75.8	79.0	77.7	77.5
linear probe CLIP	83.1	83.3	74.2	96.5	70.3	98.4	84.3
CoOp	88.5	88.5	82.0	96.1	82.4	99.0	89.4
CoCoOp	86.9	88.2	83.2	94.1	<b>82.8</b>	98.0	88.9
VP	78.5	74.8	77.9	75.5	77.8	79.7	77.4
VPT-shallow	83.5	83.8	77.5	88.6	80.9	91.2	84.2
VPT-deep	89.6	86.5	81.9	96.5	<b>82.8</b>	99.2	89.4
IVLP	85.7	89.2	81.9	<b>98.4</b>	80.3	99.2	89.1
MaPLe	86.9	88.6	83.0	97.7	82.0	99.4	89.6
DAPL	81.7	80.3	81.2	81.8	81.0	81.3	81.2
<b>PDA (Ours)</b>	<b>91.2</b>	<b>92.1</b>	<b>83.5</b>	98.1	82.5	<b>99.8</b>	<b>91.2</b>

Table 2: Comparisons with the prompt tuning methods on Office-31 dataset with ViT-B/16 as the backbone. Bold denotes the best scores.

$$z_{sa} = f_{post}\left(\text{softmax}\left(\frac{QK_{sc}^T}{\epsilon}\right)V_{sc}\right),$$

$$z_{ta} = f_{post}\left(\text{softmax}\left(\frac{QK_{tc}^T}{\epsilon}\right)V_{tc}\right),$$
(5)

where  $\epsilon$  denotes the scale value and  $T$  denotes the transpose operation. Then, we combine an add and norm module with the original visual feature, which can be formulated as:

$$z_{vs} = \frac{z_{sa} + \hat{z}}{\|z_{sa} + \hat{z}\|_2},$$

$$z_{vt} = \frac{z_{ta} + \hat{z}}{\|z_{ta} + \hat{z}\|_2},$$
(6)

where  $\|\cdot\|_2$  denotes 2-norm. Then the final augmented image representation  $\hat{z}$  can be denoted as  $\beta_1 z_{vs} + \beta_2 z_{vt}$ .

**Loss function.** Contrastive loss function is then employed to align the image representations and feature banks of source and target domains, which can be formulated as:

$$\mathcal{L}_{xa} = -\sum_i y_i^s \log \frac{\exp(\text{sim}(\hat{w}_i, h(\hat{z}^s))/t)}{\sum_{j=1}^K \exp(\text{sim}(\hat{w}_j, h(\hat{z}^s))/t)},$$
(7)

where  $h$  denotes the IFT module and  $h(\hat{z}^s)$  denotes augmented image representations of the source domain.

Similar to the base branch, we use the data of the target domain and obtain augmented image representations of the target domain  $\hat{z}^t$ . Then contrastive loss function is adopted:

$$\mathcal{L}_{ua} = -\mathbb{I}(\tau_p \geq \tau) \sum_i \hat{y}_i^t \log \frac{\exp(\text{sim}(\hat{w}_i, h(\hat{z}^t))/t)}{\sum_{j=1}^K \exp(\text{sim}(\hat{w}_j, h(\hat{z}^t))/t)}.$$
(8)

As a result, our PDA method can be trained end-to-end using a total contrastive loss:

$$\mathcal{L} = \mathcal{L}_x + \mathcal{L}_u + \gamma(\mathcal{L}_{xa} + \mathcal{L}_{ua}),$$
(9)

where  $\gamma$  is hyper-parameter. During the test phase, we calculate a weighted sum of the predictions from both the base and alignment branches, resulting in the final prediction of our model. These two branches are essential not only for enhancing model discriminability but also for aligning the distribution shift between source and target domains.

## 5 Experiments

In the following section, we describe the datasets, baselines, experimental setup, and results of our analysis. Here we show essential comparison and analysis. More details and experiments are provided in the Appendix.

### 5.1 Experimental Setting

**Datasets.** Experiments are conducted on popular benchmark datasets of unsupervised domain adaptation, namely Office-Home (Venkateswara et al. 2017), Office-31 (Saenko et al. 2010) and VisDA-2017 (Peng et al. 2018).

**Baselines.** For prompt tuning methods, we choose 7 baselines, *i.e.*, CoOp (Zhou et al. 2022b), CoCoOp (Zhou et al. 2022a), VPT (Jia et al. 2022), VP (Bahng et al. 2022), IVLP (Khattak et al. 2023), MaPLe (Khattak et al. 2023) and DAPL (Ge et al. 2022). We also compare PDA with the state-of-the-art (SOTA) methods, including ResNet-based and ViT-based methods. The ResNet-based methods are DANN (Ganin and Lempitsky 2015), JAN (Long et al. 2017), MCD (Saito et al. 2018), MDD (Zhang et al. 2019), MCC (Jin et al. 2020), SHOT (Liang, Hu, and Feng 2020)

Method	Backbone	A-C	A-P	A-R	C-A	C-P	C-R	P-A	P-C	P-R	R-A	R-C	R-P	Avg
ERM	RN50	34.9	50.0	58.0	37.4	41.9	46.2	38.5	31.2	60.4	53.9	41.2	59.9	46.1
DANN		45.6	59.3	70.1	47.0	58.5	60.9	46.1	43.7	68.5	63.2	51.8	76.8	57.6
JAN		45.9	61.2	68.9	50.4	59.7	61.0	45.8	43.4	70.3	63.9	52.4	76.8	58.3
MDD		54.9	73.7	77.8	60.0	71.4	71.8	61.2	53.6	78.1	72.5	60.2	82.3	68.1
SHOT		<b>57.1</b>	78.1	81.5	68.0	78.2	78.1	67.4	54.9	82.2	73.3	<b>58.8</b>	84.3	71.8
CDAN w/ SDAT		56.0	72.2	78.6	62.5	73.2	71.8	62.1	55.9	80.3	75.0	61.4	84.5	69.5
<b>PDA (Ours)</b>		55.4	<b>85.1</b>	<b>85.8</b>	<b>75.2</b>	<b>85.2</b>	<b>85.2</b>	<b>74.2</b>	<b>55.2</b>	<b>85.8</b>	<b>74.7</b>	55.8	<b>86.3</b>	<b>75.3</b>
TVT	ViT	74.9	86.8	89.5	82.8	87.9	88.3	79.8	71.9	90.1	85.5	74.6	90.6	83.6
SSRT		<b>75.2</b>	89.0	91.1	85.1	88.3	89.9	85.0	<b>74.2</b>	91.2	85.7	<b>78.6</b>	91.8	85.4
Deit-based		61.8	79.5	84.3	75.4	78.8	81.2	72.8	55.7	84.4	78.3	59.3	86.0	74.8
CDTrans-Deit		68.8	85.0	86.9	81.5	87.1	87.3	79.6	63.3	88.2	82.0	66.0	90.6	80.5
CDAN w/ SDAT		69.1	86.6	88.9	81.9	86.2	88.0	81.0	66.7	89.7	86.2	72.1	91.9	82.4
<b>PDA (Ours)</b>		73.5	<b>91.4</b>	<b>91.3</b>	<b>86.0</b>	<b>91.6</b>	<b>91.5</b>	<b>86.0</b>	73.5	<b>91.7</b>	<b>86.4</b>	73.0	<b>92.4</b>	<b>85.7</b>

Table 3: Comparisons with SOTA methods on Office-Home with ResNet50 and ViT as the backbone. Bold is the best scores.

Method	Backbone	plane	bicycle	bus	car	horse	knife	mcycl	person	plant	sktbrd	train	truck	Avg
ERM	RN101	55.1	53.3	61.9	59.1	80.6	17.9	79.7	31.2	81.0	26.5	73.5	8.5	52.4
DANN		81.9	77.7	82.8	44.3	81.2	29.5	65.1	28.6	51.9	54.6	82.8	7.8	57.4
MCD		87.0	60.9	83.7	64.0	88.9	79.6	84.7	76.9	88.6	40.3	83.0	25.8	71.9
MCC		88.1	<b>80.3</b>	80.5	71.5	90.1	<b>93.2</b>	85.0	71.6	89.4	73.8	85.0	36.9	78.8
SHOT		94.3	<b>88.5</b>	80.1	57.3	93.1	94.9	80.7	80.3	91.5	89.1	86.3	58.2	82.9
CDAN w/ SDAT		94.8	77.1	82.8	60.9	92.3	95.2	91.7	<b>79.9</b>	<b>89.9</b>	<b>91.2</b>	88.5	41.2	82.1
<b>PDA (Ours)</b>		<b>97.2</b>	82.3	<b>89.4</b>	<b>76.0</b>	<b>97.4</b>	87.5	<b>95.8</b>	79.6	87.2	89.0	<b>93.3</b>	<b>62.1</b>	<b>86.4</b>
TVT	ViT	92.9	85.6	77.5	60.5	93.6	98.2	89.3	76.4	93.6	92.0	91.7	55.7	83.9
SSRT		98.9	87.6	89.1	<b>84.8</b>	98.3	98.7	96.3	81.1	94.8	<b>97.9</b>	94.5	43.1	88.8
Deit-based		98.2	73.0	82.5	62.0	97.3	63.5	<b>96.5</b>	29.8	68.7	86.7	<b>96.7</b>	23.6	73.2
CDTrans-Deit		97.1	90.5	82.4	77.5	96.6	96.1	93.6	<b>88.6</b>	<b>97.9</b>	86.9	90.3	62.8	88.4
CDAN w/ SDAT		96.3	80.7	74.5	65.4	95.8	<b>99.5</b>	92.0	83.7	93.6	88.9	85.8	57.2	84.5
<b>PDA (Ours)</b>		<b>99.2</b>	<b>91.1</b>	<b>91.9</b>	77.1	<b>98.4</b>	93.6	95.1	84.9	87.2	97.3	95.3	<b>65.3</b>	<b>89.7</b>

Table 4: Comparisons with SOTA methods on VisDA-2017 with ResNet101 and ViT as the backbone. Bold is the best scores.

and SDAT (Rangwani et al. 2022), and the ViT-based methods are Deit (Touvron et al. 2021), CDTrans (Xu et al. 2022), SDAT, SSRT (Sun et al. 2022) and TVT (Yang et al. 2023).

**Experimental Setup.** We adopt ResNet50 (He et al. 2016), ResNet101 and ViT-B/16 (Dosovitskiy et al. 2021) as our backbones. Following Zhou et al. (Zhou et al. 2022b), we adopt text prompt as prompt design for ResNet-based backbone. Following Khattak et al. (Khattak et al. 2023), we adopt the multi-modal prompt as prompt design for the ViT-based backbone. The parameters in the encoders of CLIP are fixed, and we train the prompt and IFT module using the SGD optimizer for 10 epochs on the Office-Home and VisDA-2017 datasets, and for 20 epochs on the Office-31 dataset, with a batch size of 32. For all prompt tuning methods, we set the learning rate initially to around 0.003 initially and decay it using a cosine annealing rule. Moreover, the context tokens length is set to 2 for MaPLe and our PDA method, 10 for VPT and VP, and 16 for CoOp and CoCoOp.

## 5.2 Comparisons with Prompt Tuning Methods

**Results on Office-Home.** As shown in Table 1, our PDA achieves the best performance on almost all tasks with 85.7% accuracy, and achieves an average accuracy improvement of 3.6%, 1.8%, and 1.5%, respectively, compared with zero-shot CLIP, CoOp and MaPLe. For some tasks, such as

C-A and P-A, we observe improvements of around 4.0% compared with MaPLe. Furthermore, we find that multi-modal prompt tuning methods perform better than single-modal prompt tuning methods.

**Results on Office-31.** As shown in Table 2, our PDA method also outperforms all other prompt tuning methods. We observe that prompt tuning can significantly improve the transferability of zero-shot CLIP, as PDA outperforms zero-shot CLIP by 13.7% on average accuracy. For some tasks, such as W-D and D-W, our PDA outperforms zero-shot CLIP by 22.1% and 22.3%, respectively, indicating that the domain shift problem is well alleviated.

## 5.3 Comparisons with SOTA Methods

**Results on Office-Home.** Table 3 shows the quantitative comparison with the ResNet-based and ViT-based methods. PDA outperforms other SOTA methods with identical backbones. For instance, with ResNet50 as the backbone, PDA outperforms SHOT by 3.5% and SDAT by 5.8% by a large margin, respectively. With ViT as the backbone, PDA outperforms SSRT by 0.3% and TVT by 2.1%, respectively. Compared with these unimodal methods, PDA exhibits superior performance with multi-modal interaction.

**Results on VisDA-2017.** Table 4 shows the experimental results on the VisDA-2017 dataset. Our PDA method also



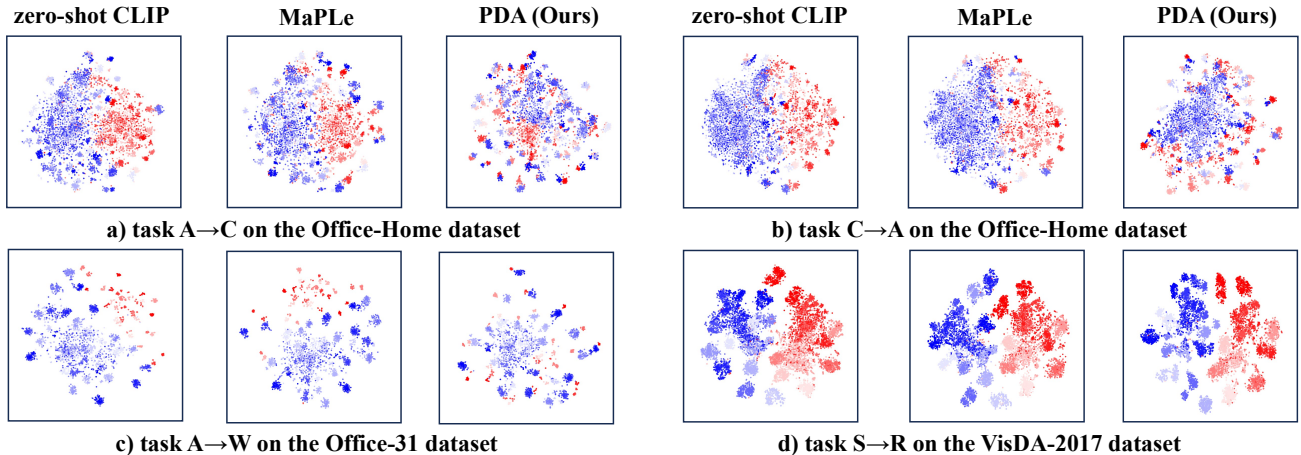


Figure 3: The t-SNE visualization for different tasks on the three datasets with zero-shot CLIP, MaPLe and our PDA method. Image features extracted from the source and target domain are shown in blue and red, respectively.

achieves SOTA performance on the VisDA-2017 dataset with different backbones. For example, PDA outperforms SHOT and SDAT by a large margin of 3.5% and 4.3%, respectively. With ResNet101 as the backbone, PDA outperforms SSRT by 1.1% and TVT by 5.8%, respectively.

#### 5.4 Ablation Study

**Effect of each constraint loss.** Table 5 shows the experimental results of integrating different constraint losses. In most cases, each constraint loss contributes positively to enhancing the model’s performance. For Office-Home dataset, we observe a consistent performance improvement with the introduction of each constraint loss, and the combination of them improves the averaged results by 3.6%. For Office-31 dataset, a notable improvement of 12.1% is achieved by incorporating the  $\mathcal{L}_x$ , which ensures discrimination among different classes. The combined influence of these constraint losses results in an impressive average performance improvement of 13.7%. For VisDA-2017 dataset, we encounter a tendency towards overfitting to data of source domain when employing  $\mathcal{L}_x$ , but this issue is mitigated by the application of other constraint losses.

$\mathcal{L}_x$	$\mathcal{L}_{xa}$	$\mathcal{L}_u$	$\mathcal{L}_{ua}$	OfficeHome	Office31	VisDA17
				82.1	77.5	88.9
✓				84.2 (+2.1)	89.6 (+12.1)	83.5 (-5.4)
✓	✓			84.6 (+2.5)	89.8 (+12.3)	85.2 (-3.7)
✓	✓	✓		85.2 (+3.1)	90.5 (+13.0)	89.0 (+0.1)
✓	✓	✓	✓	<b>85.7 (+3.6)</b>	<b>91.2 (+13.7)</b>	<b>89.7 (+0.8)</b>

Table 5: Ablation on different constraint losses. The average results of three datasets are reported. Improvements over the baseline of CLIP are marked in green.

**Sensitivity analysis of the pseudo label threshold  $\tau$  and context token length.** Figure 4 presents the results of varying the context token length and pseudo label threshold, respectively. The results suggest that the performance of our method is generally robust to both of them.

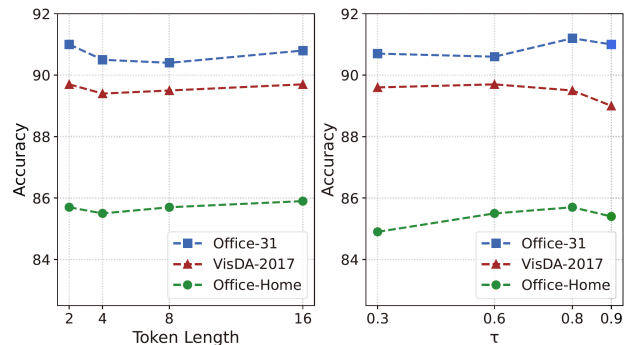


Figure 4: Sensitivity analysis of the context token length (left) and pseudo label threshold  $\tau$  (right) on three datasets.

#### 5.5 Visualization

As shown in Figure 3, we visualize the image features extracted from zero-shot CLIP, MaPLe and our PDA on four tasks from the three datasets via t-SNE. We can observe that our PDA method can better align the two domains.

## 6 Conclusion

In this paper, we demonstrate the effectiveness of vision language models and prompt tuning of VLMs for unsupervised domain adaptation. Based on this, we introduce distribution alignment into prompt tuning and propose a Prompt-based Distribution Alignment (PDA) method with a two-branch training paradigm. These two branches play a vital role not only in improving model discriminability but also in mitigating the distribution shift between the source and target domains. Extensive experiments confirm the effectiveness of our proposed method and our PDA method achieves new state-of-the-art performance for unsupervised domain adaptation. Due to the transferability of the learned prompts, we may further explore prompt alignment for unsupervised domain adaptation or other downstream tasks in future work.

## Acknowledgments

This work was supported by the National Natural Science Foundation of China under grant number U21A20485, 62088102, and NSFC General Program under grant number 62176215.

## References

- Bahng, H.; Jahanian, A.; Sankaranarayanan, S.; and Isola, P. 2022. Exploring Visual Prompts for Adapting Large-Scale Models. arXiv:2203.17274.
- Bai, S.; Zhou, W.; Luan, Z.; Wang, D.; and Badong, C. 2024. Improving Cross-domain Few-shot Classification with Multilayer Perceptron. In *ICASSP 2024-2024 IEEE International Conference on Acoustics, Speech and Signal Processing (ICASSP)*. IEEE.
- Chen, Z.; Ge, J.; Zhan, H.; Huang, S.; and Wang, D. 2021. Pareto Self-Supervised Training for Few-Shot Learning. In *Proceedings of the IEEE/CVF Conference on Computer Vision and Pattern Recognition*, 13663–13672.
- Chen, Z.; Xiao, T.; and Kuang, K. 2022. BA-GNN: On Learning Bias-Aware Graph Neural Network. In *2022 IEEE 38th International Conference on Data Engineering (ICDE)*, 3012–3024. IEEE.
- Dosovitskiy, A.; Beyer, L.; Kolesnikov, A.; Weissenborn, D.; Zhai, X.; Unterthiner, T.; Dehghani, M.; Minderer, M.; Heigold, G.; Gelly, S.; et al. 2021. An image is worth 16x16 words: Transformers for image recognition at scale. *International Conference on Learning Representations*.
- Ganin, Y.; and Lempitsky, V. 2015. Unsupervised domain adaptation by backpropagation. In *International conference on machine learning*, 1180–1189. PMLR.
- Gao, P.; Geng, S.; Zhang, R.; Ma, T.; Fang, R.; Zhang, Y.; Li, H.; and Qiao, Y. 2021. CLIP-Adapter: Better Vision-Language Models with Feature Adapters. arXiv:2110.04544.
- Ge, C.; Huang, R.; Xie, M.; Lai, Z.; Song, S.; Li, S.; and Huang, G. 2022. Domain Adaptation via Prompt Learning. arXiv:2202.06687.
- Guo, Z.; Zhang, R.; Qiu, L.; Ma, X.; Miao, X.; He, X.; and Cui, B. 2023. CALIP: Zero-Shot Enhancement of CLIP with Parameter-Free Attention. *Proceedings of the AAAI Conference on Artificial Intelligence*, 37(1): 746–754.
- He, K.; Zhang, X.; Ren, S.; and Sun, J. 2016. Deep residual learning for image recognition. In *Proceedings of the IEEE conference on computer vision and pattern recognition*, 770–778.
- Huang, Z.; Zeng, Z.; Huang, Y.; Liu, B.; Fu, D.; and Fu, J. 2021. Seeing Out of the Box: End-to-End Pre-training for Vision-Language Representation Learning. In *The IEEE Conference on Computer Vision and Pattern Recognition*.
- Jia, C.; Yang, Y.; Xia, Y.; Chen, Y.-T.; Parekh, Z.; Pham, H.; Le, Q.; Sung, Y.-H.; Li, Z.; and Duerig, T. 2021. Scaling up visual and vision-language representation learning with noisy text supervision. In *International conference on machine learning*, 4904–4916. PMLR.
- Jia, M.; Tang, L.; Chen, B.-C.; Cardie, C.; Belongie, S.; Hariharan, B.; and Lim, S.-N. 2022. Visual prompt tuning. In *Proceedings of the 17th European Conference on Computer Vision*, 709–727. Springer.
- Jin, Y.; Wang, X.; Long, M.; and Wang, J. 2020. Minimum class confusion for versatile domain adaptation. In *Proceedings of the 16th European conference on Computer vision*, 464–480. Springer.
- Khattak, M. U.; Rasheed, H.; Maaz, M.; Khan, S.; and Khan, F. S. 2023. Maple: Multi-modal prompt learning. In *Proceedings of the IEEE Conference on Computer Vision and Pattern Recognition*, 19113–19122.
- Kim, W.; Son, B.; and Kim, I. 2021. Vilt: Vision-and-language transformer without convolution or region supervision. In *International Conference on Machine Learning*, 5583–5594. PMLR.
- Liang, J.; Hu, D.; and Feng, J. 2020. Do we really need to access the source data? source hypothesis transfer for unsupervised domain adaptation. In *International conference on machine learning*, 6028–6039. PMLR.
- Long, M.; Cao, Y.; Wang, J.; and Jordan, M. 2015. Learning transferable features with deep adaptation networks. In *International conference on machine learning*, 97–105. PMLR.
- Long, M.; Cao, Z.; Wang, J.; and Jordan, M. I. 2018. Conditional adversarial domain adaptation. *Advances in neural information processing systems*, 31.
- Long, M.; Zhu, H.; Wang, J.; and Jordan, M. I. 2017. Deep transfer learning with joint adaptation networks. In *International conference on machine learning*, 2208–2217. PMLR.
- Peng, X.; Usman, B.; Kaushik, N.; Wang, D.; Hoffman, J.; and Saenko, K. 2018. Visda: A synthetic-to-real benchmark for visual domain adaptation. In *Proceedings of the IEEE Conference on Computer Vision and Pattern Recognition Workshops*, 2021–2026.
- Pfeiffer, J.; Ruder, S.; Vulić, I.; and Ponti, E. M. 2023. Modular Deep Learning. arXiv:2302.11529.
- Radford, A.; Kim, J. W.; Hallacy, C.; Ramesh, A.; Goh, G.; Agarwal, S.; Sastry, G.; Askell, A.; Mishkin, P.; Clark, J.; et al. 2021. Learning transferable visual models from natural language supervision. In *International conference on machine learning*, 8748–8763. PMLR.
- Rangwani, H.; Aithal, S. K.; Mishra, M.; Jain, A.; and Radhakrishnan, V. B. 2022. A closer look at smoothness in domain adversarial training. In *International Conference on Machine Learning*, 18378–18399. PMLR.
- Saenko, K.; Kulis, B.; Fritz, M.; and Darrell, T. 2010. Adapting visual category models to new domains. In *Proceedings of the 11th European conference on Computer vision: Part IV*, 213–226. Springer.
- Saito, K.; Watanabe, K.; Ushiku, Y.; and Harada, T. 2018. Maximum classifier discrepancy for unsupervised domain adaptation. In *Proceedings of the IEEE conference on computer vision and pattern recognition*, 3723–3732.
- Sun, B.; Feng, J.; and Saenko, K. 2016. Return of Frustratingly Easy Domain Adaptation. *Proceedings of the AAAI Conference on Artificial Intelligence*, 30(1).



- Sun, T.; Lu, C.; Zhang, T.; and Ling, H. 2022. Safe self-refinement for transformer-based domain adaptation. In *Proceedings of the IEEE conference on computer vision and pattern recognition*, 7191–7200.
- Tan, H.; and Bansal, M. 2019. LXMERT: Learning Cross-Modality Encoder Representations from Transformers. In *Proceedings of the 2019 Conference on Empirical Methods in Natural Language Processing*.
- Tang, H.; Chen, K.; and Jia, K. 2020. Unsupervised domain adaptation via structurally regularized deep clustering. In *Proceedings of the IEEE conference on computer vision and pattern recognition*, 8725–8735.
- Touvron, H.; Cord, M.; Douze, M.; Massa, F.; Sablayrolles, A.; and Jégou, H. 2021. Training data-efficient image transformers & distillation through attention. In *International conference on machine learning*, 10347–10357. PMLR.
- Venkateswara, H.; Eusebio, J.; Chakraborty, S.; and Panchanathan, S. 2017. Deep hashing network for unsupervised domain adaptation. In *Proceedings of the IEEE conference on computer vision and pattern recognition*, 5018–5027.
- Wilson, G.; and Cook, D. J. 2020. A survey of unsupervised deep domain adaptation. *ACM Transactions on Intelligent Systems and Technology (TIST)*, 11(5): 1–46.
- Xiao, T.; Chen, Z.; Guo, Z.; Zhuang, Z.; and Wang, S. 2022. Decoupled self-supervised learning for graphs. *Advances in Neural Information Processing Systems*, 35: 620–634.
- Xiao, T.; Chen, Z.; Wang, D.; and Wang, S. 2021. Learning how to propagate messages in graph neural networks. In *Proceedings of the 27th ACM SIGKDD Conference on Knowledge Discovery & Data Mining*, 1894–1903.
- Xu, T.; Chen, W.; Wang, P.; Wang, F.; Li, H.; and Jin, R. 2022. Cdtrans: Cross-domain transformer for unsupervised domain adaptation. *International Conference on Learning Representations*.
- Yang, J.; Liu, J.; Xu, N.; and Huang, J. 2023. Tvt: Transferable vision transformer for unsupervised domain adaptation. In *Proceedings of the IEEE/CVF Winter Conference on Applications of Computer Vision*, 520–530.
- Zhang, M.; Huang, S.; Li, W.; and Wang, D. 2022a. Tree structure-aware few-shot image classification via hierarchical aggregation. In *European Conference on Computer Vision, ECCV*, 453–470. Springer.
- Zhang, M.; Huang, S.; and Wang, D. 2022. Domain generalized few-shot image classification via meta regularization network. In *ICASSP 2022-2022 IEEE International Conference on Acoustics, Speech and Signal Processing (ICASSP)*, 3748–3752. IEEE.
- Zhang, M.; Wang, D.; and Gai, S. 2020. Knowledge distillation for model-agnostic meta-learning. In *ECAI 2020*, 1355–1362. IOS Press.
- Zhang, M.; Yuan, J.; He, Y.; Li, W.; Chen, Z.; and Kuang, K. 2023a. MAP: Towards Balanced Generalization of IID and OOD through Model-Agnostic Adapters. In *Proceedings of the IEEE/CVF International Conference on Computer Vision*, 11921–11931.
- Zhang, M.; Zhuang, Z.; Wang, Z.; Wang, D.; and Li, W. 2023b. RotoGBML: Towards Out-of-Distribution Generalization for Gradient-Based Meta-Learning. *arXiv preprint arXiv:2303.06679*.
- Zhang, R.; Zhang, W.; Fang, R.; Gao, P.; Li, K.; Dai, J.; Qiao, Y.; and Li, H. 2022b. Tip-adapter: Training-free adaptation of clip for few-shot classification. In *European Conference on Computer Vision*, 493–510. Springer.
- Zhang, Y.; Liu, T.; Long, M.; and Jordan, M. 2019. Bridging theory and algorithm for domain adaptation. In *International conference on machine learning*, 7404–7413. PMLR.
- Zhou, K.; Yang, J.; Loy, C. C.; and Liu, Z. 2022a. Conditional prompt learning for vision-language models. In *Proceedings of the IEEE Conference on Computer Vision and Pattern Recognition*, 16816–16825.
- Zhou, K.; Yang, J.; Loy, C. C.; and Liu, Z. 2022b. Learning to prompt for vision-language models. *International Journal of Computer Vision*, 130(9): 2337–2348.
- Zhu, D.; Li, Y.; Shao, Y.; Hao, J.; Wu, F.; Kuang, K.; Xiao, J.; and Wu, C. 2023a. Generalized Universal Domain Adaptation with Generative Flow Networks. *arXiv preprint arXiv:2305.04466*.
- Zhu, D.; Li, Y.; Zhang, M.; Yuan, J.; Liu, J.; Kuang, K.; and Wu, C. 2023b. Bridging the Gap: Neural Collapse Inspired Prompt Tuning for Generalization under Class Imbalance. *arXiv preprint arXiv:2306.15955*.

## Supplementary Material

This appendix is organized as follows:

- Section A provides the detailed dataset information.
- Section B provides the detailed additional training implementation details.
- Section C gives additional experiment results, including additional comparison with prompt tuning methods and SOTA methods, additional visualization, and the analysis of the metrics that measure the performance.

### A Dataset Details

**Office-31** (Saenko et al. 2010). The Office-31 dataset is a popular small-scaled benchmark for domain adaptation. It consists of 4,110 images of 31 categories, with three distinct domains: Amazon (A), Webcam (W), and DSLR (D). In our experiment, we conduct 6 unsupervised domain adaptation (UDA) tasks, such as  $A \rightarrow D$ ,  $A \rightarrow W$ , and so on.

**Office-Home** (Venkateswara et al. 2017). The Office-Home dataset is a medium-scaled benchmark for domain adaptation. It contains a total of 15,500 images from four distinct domains: Art (A), Clip Art (C), Product (P), and Real World (R). Each domain contains objects from 65 categories commonly found in office and home environments. To evaluate the effectiveness of our proposed method, we conduct 12 unsupervised domain adaptation (UDA) tasks, which involve adapting models trained on a source domain to a target domain, for example,  $A \rightarrow C$ ,  $A \rightarrow P$ , and so on.

**VisDA-2017** (Peng et al. 2018). The Visual Domain Adaptation Challenge 2017 (VisDA17) dataset is a more challenging large-scaled benchmark for synthetic-to-real domain adaptation. It consists of 12 categories, with a total of 152,397 synthetic images generated by rendering 3D models from different angles and light conditions, and 55,388 real-world images collected from the Microsoft Common Objects in Context (MSCOCO) dataset. In our experiments, we follow the setting of (Ge et al. 2022) and treat the synthetic images as the source domain and the real-world images as the target domain, *i.e.*,  $S \rightarrow R$ .

### B Implementation Details

We adopt the pre-trained CLIP model with ResNet50, ResNet101 and ViT-B/16 as our backbones. For all prompt tuning methods, we fix the parameters in the encoders and the prompt is trained with the SGD optimizer for 10 epochs for Office-Home and VisDA-2017 datasets, 20 epochs for Office-31 dataset, where the batch size is 32. Referring to the original paper, the learning rate is set to 0.001 for CoCoOp, 0.0025 for VPT and VP, 0.003 for CoOp, DAPL and our PDA method, and 0.0035 for IVLP and MaPLe. The pseudo labeling threshold  $\tau$  is set to 0.8 for Office-Home, 0.8 for Office-31 and 0.6 for VisDA-2017 dataset. The weight  $\gamma$  of constraint losses is set to 1.0. The weights  $\beta_1, \beta_2$  of the enhanced augmented image features are set to 0.1 and 0.1. For N-way K-shot feature banks, N is set to the number of classes in each dataset, and K is set to 5.

For the Office-Home and VisDA-2017 datasets, we utilize the logits of zero-shot CLIP to generate pseudo labels due to

their high average accuracy with zero-shot CLIP. However, for the Office-31 dataset, the average accuracy of zero-shot CLIP is lower. Therefore, we apply a warm-up strategy, in which we use the logits of zero-shot CLIP for the first couple of epochs and leverage the logits of prompt tuning CLIP for the last couple of epochs. If the accuracy is still lower, we only use pseudo labels for the last few epochs.

### C Supplement Comparison Experiments

The supplement experiments mainly demonstrate the effectiveness of our PDA method across different backbones. Furthermore, to give a more detailed analysis, we conduct an additional ablation study, additional visualization experiments, and a metric analysis of our PDA method.

#### C.1 Comparisons with Prompt Tuning Methods

**Results on Office-Home.** As shown in Table 6, we observe a stable improvement in performance across 12 tasks with different backbones on the Office-Home dataset, and our method achieves state-of-the-art performance among all prompt tuning methods.

**Results on VisDA-2017.** Table 7 shows the experimental results on the VisDA-2017 dataset and demonstrates PDA also achieves state-of-the-art performance among all prompt tuning methods. Our observations indicate that most prompt tuning methods exhibit inferior performance compared to the zero-shot CLIP model, primarily due to the issue of overfitting. Interestingly, we also find an overfitting problem with the ResNet101 and Deit models, suggesting that the prompt has a similar characteristic to the model parameters. Therefore, to learn an effective prompt, it is necessary to develop an appropriate training strategy to avoid overfitting problem.

**Results on Office-31.** Table 8 presents the experimental results on the Office-31 dataset. Our proposed PDA method significantly improves the transferability compared to zero-shot CLIP, and our PDA method achieves state-of-the-art performance among all prompt tuning methods. The experimental results demonstrate the effectiveness of our proposed PDA method.

#### C.2 Comparisons with SOTA Methods

Table 10 shows the experimental results on the Office-31 dataset. PDA outperforms most of the SOTA methods. We observe that both the ResNet50 and Deit-based models outperform the zero-shot CLIP, suggesting that the CLIP-based model may be inadequate in handling relatively small domain shift problem. This highlights the efficacy of the conventional transfer learning approach employed by unimodal models in adapting more effectively to the data. However, the prompt tuning methods can significantly improve the performance of CLIP model, enabling it to compare favorably with these state-of-the-art UDA methods with much fewer parameters.

#### C.3 Analyzing the Metrics

Table 9 summarizes the quantitative results of three methods. We evaluate the inner-class distance  $D_1$  and variance, which are defined as the averaged  $L_2$  distance and variance

Method	Backbone	A-C	A-P	A-R	C-A	C-P	C-R	P-A	P-C	P-R	R-A	R-C	R-P	Avg
zero-shot CLIP	RN50	51.7	81.5	82.3	71.7	81.5	82.3	71.7	51.7	82.3	71.7	51.7	81.5	71.8
linear probe CLIP		32.3	40.3	52.7	40.1	50.0	50.1	49.3	35.0	71.7	61.5	37.6	74.4	49.6
CoOp		53.8	84.6	84.1	71.0	83.1	82.3	70.4	53.8	83.6	74.2	54.6	<b>87.0</b>	73.5
CoCoOp		52.1	84.6	84.9	72.0	85.1	84.0	69.3	54.3	84.5	72.6	53.2	86.8	73.6
VP		51.8	81.6	82.6	71.9	81.7	82.5	71.8	51.0	82.6	72.0	51.5	81.7	71.9
DAPL		54.1	84.3	84.8	74.4	83.7	85.0	74.5	54.6	84.8	75.2	54.7	83.8	74.5
<b>PDA (Ours)</b>		<b>55.4</b>	<b>85.1</b>	<b>85.8</b>	<b>75.2</b>	<b>85.2</b>	<b>85.2</b>	<b>74.2</b>	<b>55.2</b>	<b>85.8</b>	<b>74.7</b>	<b>55.8</b>	86.3	<b>75.3</b>
zero-shot CLIP	RN101	56.1	85.8	85.3	77.2	85.8	85.3	77.2	56.1	85.3	77.2	56.1	85.8	76.1
linear probe CLIP		38.7	47.4	57.5	52.1	60.5	59.7	55.8	45.9	76.1	69.0	48.2	78.7	57.5
CoOp		59.7	86.6	87.0	76.6	85.7	85.9	77.0	<b>61.0</b>	86.5	79.2	60.6	88.6	77.9
CoCoOp		59.1	86.6	86.8	77.0	87.7	86.2	76.3	60.2	87.1	79.4	59.8	88.4	77.9
VP		55.6	86.1	85.3	76.1	86.1	85.5	76.6	55.8	85.5	76.1	56.0	86.1	75.9
DAPL		59.0	<b>88.1</b>	87.5	79.6	87.9	87.1	79.6	58.8	87.2	<b>79.8</b>	58.8	88.0	78.5
<b>PDA (Ours)</b>		<b>60.9</b>	87.5	<b>87.9</b>	<b>79.8</b>	<b>88.6</b>	<b>87.6</b>	<b>80.0</b>	60.4	<b>87.7</b>	79.7	<b>61.2</b>	<b>88.9</b>	<b>79.2</b>

Table 6: Comparisons with the prompt tuning methods. Top-1 classification accuracies on Office-Home dataset with ResNet50 and ResNet101 as the backbone. Bold denotes the best scores.

Method	Backbone	plane	bicycle	bus	car	horse	knife	mcycl	person	plant	sktbrd	train	truck	Avg
zero-shot CLIP	RN101	98.1	83.7	90.8	74.2	97.3	85.8	95.2	69.4	82.1	<b>90.0</b>	92.5	61.1	85.0
linear probe CLIP		77.1	38.2	63.0	72.7	80.4	10.3	97.7	13.6	<b>89.5</b>	70.5	<b>96.1</b>	4.2	59.4
CoOp		97.1	<b>86.3</b>	92.0	67.5	97.3	49.1	92.6	51.0	88.9	78.7	93.0	33.3	77.2
CoCoOp		96.5	75.0	<b>94.1</b>	58.4	<b>98.3</b>	59.3	<b>96.1</b>	62.9	88.4	85.5	88.6	67.0	80.8
VP		<b>98.2</b>	84.4	90.1	74.8	96.5	85.3	94.1	72.1	82.6	89.0	92.5	59.7	84.9
DAPL		98.1	83.9	90.9	75.1	97.6	87.1	95.2	75.7	84.8	90.7	91.8	61.7	86.1
<b>PDA (Ours)</b>		97.2	82.3	89.4	<b>76.0</b>	97.4	<b>87.5</b>	95.8	<b>79.6</b>	87.2	89.0	93.3	<b>62.1</b>	<b>86.4</b>
zero-shot CLIP	ViT	<b>99.2</b>	92.2	93.5	76.7	98.3	90.4	94.6	83.6	85.4	96.1	94.3	62.5	88.9
linear probe CLIP		91.4	56.9	74.8	55.1	52.3	23.3	92.5	7.6	88.9	84.9	90.7	3.4	60.2
CoOp		98.7	89.8	94.2	69.7	<b>99.0</b>	71.5	96.3	53.9	<b>91.5</b>	96.3	95.8	35.7	82.7
CoCoOp		99.1	92.4	92.0	71.7	99.1	<b>95.0</b>	95.8	22.7	90.3	95.6	96.0	60.6	84.2
VP		99.0	91.2	<b>93.8</b>	77.0	98.3	89.1	94.4	85.7	82.9	95.1	94.1	63.8	88.7
VPT-shallow		99.0	86.8	95.7	69.3	98.5	73.0	96.5	78.3	80.3	96.2	93.4	56.1	85.3
VPT-deep		98.7	78.2	96.0	68.7	98.8	83.6	<b>97.0</b>	82.5	87.4	94.5	94.3	54.6	86.2
IVLP		98.6	86.8	88.5	76.0	97.5	68.3	95.7	59.0	90.5	94.5	<b>97.9</b>	36.3	82.5
MaPLe		98.6	85.8	93.0	68.8	99.2	72.4	96.8	77.1	84.7	96.0	95.9	33.1	83.5
DAPL		99.1	<b>92.6</b>	93.1	<b>77.4</b>	98.4	92.2	94.6	84.7	88.3	96.1	93.7	63.4	89.5
<b>PDA (Ours)</b>	<b>99.2</b>	91.1	91.9	77.1	98.4	93.6	95.1	<b>84.9</b>	87.2	<b>97.3</b>	95.3	<b>65.3</b>	<b>89.7</b>	

Table 7: Comparisons with the prompt tuning methods. Top-1 classification accuracies on VisDA-2017 dataset with ResNet101 and ViT-B/16 as the backbone. Bold denotes the best scores.

Method	Backbone	A-D	A-W	D-A	D-W	W-A	W-D	Avg
zero-shot CLIP	RN50	74.1	67.0	72.8	67.0	72.8	74.1	71.3
linear probe CLIP		75.3	70.4	45.7	64.4	54.4	81.1	65.2
CoOp		82.3	78.2	<b>77.9</b>	90.7	76.3	96.4	83.6
CoCoOp		82.9	76.7	75.6	88.8	76.7	93.6	82.4
VP		74.9	68.4	73.9	68.4	74.1	76.1	72.6
DAPL		77.3	71.9	76.7	74.7	<b>77.4</b>	79.7	76.3
<b>PDA (Ours)</b>		<b>85.1</b>	<b>81.1</b>	76.6	<b>92.8</b>	77.3	<b>97.8</b>	<b>85.1</b>
zero-shot CLIP	RN101	78.7	77.2	73.7	77.1	73.8	78.7	76.5
linear probe CLIP		79.7	77.6	49.8	66.7	59.2	86.1	69.9
CoOp		85.5	85.3	81.5	92.7	79.3	<b>97.4</b>	87.0
CoCoOp		84.5	83.6	80.5	93.1	<b>80.3</b>	96.8	86.5
VP		79.1	78.2	74.2	78.0	74.7	78.5	77.1
DAPL		83.9	81.0	78.1	83.5	78.6	82.7	81.3
<b>PDA (Ours)</b>		<b>90.4</b>	<b>86.9</b>	<b>81.7</b>	<b>96.0</b>	79.9	<b>97.4</b>	<b>88.7</b>

Table 8: Comparisons with the prompt tuning methods. Top-1 classification accuracies on Office-31 dataset with ResNet50 and ResNet101 as the backbone. Bold denotes the best scores.

Feature Type	Method	zero-shot CLIP		MaPLE		PDA (Ours)	
	domain	source	target	source	target	source	target
	accuracy ( $\uparrow$ )	-	67.6	-	72.2	-	<b>73.5</b>
Text Feature	inner-class L2 distance ( $\downarrow$ )	0.000		0.000		0.000	
	inner-class variance ( $\downarrow$ )	0.002		0.002		0.002	
	<b>inter-class L2 distance (<math>\uparrow</math>)</b>	0.685		0.595		<b>0.688</b>	
Image Feature	inner-class L2 distance ( $\downarrow$ )	0.554	0.441	0.560	0.462	<b>0.416</b>	<b>0.379</b>
	inner-class variance ( $\downarrow$ )	0.002	0.002	0.002	0.002	0.002	0.002
	inter-class L2 distance ( $\uparrow$ )	0.717	0.625	<b>0.744</b>	<b>0.717</b>	0.605	0.627
	$r$ ( $\uparrow$ )	1.294	1.417	1.329	1.552	<b>1.454</b>	<b>1.654</b>
	MMD ( $\downarrow$ )		0.307		0.260		<b>0.171</b>
	KL divergence ( $\downarrow$ )		32.214		29.601		<b>28.517</b>

Table 9: Quantitative analysis of text and image features learned by zero-shot CLIP, MaPLE and PDA on Office-Home with ViT-B/16 backbone. The source domain is art, and the target domain is clipart. Bold denotes best scores.

Method		A-D	A-W	D-A	D-W	W-A	W-D	Avg
ERM	RN50	68.9	68.4	62.5	96.7	60.7	99.3	76.1
DANN		79.7	82.0	68.2	96.9	67.4	99.1	82.2
JAN		84.7	85.4	68.6	97.4	70.0	99.8	84.3
MCD		<b>92.2</b>	<b>88.6</b>	69.5	<b>98.5</b>	69.7	<b>100.0</b>	<b>86.5</b>
zero-shot CLIP		74.1	67.0	72.8	67.0	72.8	74.1	71.3
<b>PDA (Ours)</b>		85.1	81.1	<b>76.6</b>	92.8	<b>77.3</b>	97.8	<u>85.1</u>
Deit-based	ViT	88.7	89.2	80.1	98.9	79.8	100.0	89.5
CDTrans-Deit		<b>97.0</b>	<b>96.7</b>	81.1	<b>99.0</b>	81.9	<b>100.0</b>	<b>92.6</b>
zero-shot CLIP		77.7	75.8	79.0	75.8	79.0	77.7	77.5
<b>PDA (Ours)</b>		91.2	92.1	<b>83.5</b>	98.1	<b>82.5</b>	99.8	<u>91.2</u>

Table 10: Comparisons with SOTA methods. Top-1 classification accuracies on Office-31 dataset with ResNet50 and ViT as the backbone. Bold denotes the best scores and underscore denotes the second-best result.

for inner-class features, respectively. Moreover, we evaluate the inter-class distance  $D_2$ , which is the average  $L_2$  distance between the learned representations of each class and the centroid of other classes. We also define a ratio  $r$  between the average of the inter-class distance and the inner-class distance, i.e.,  $r = D_2/D_1$ , which denotes the compactness of the representations in each class.

	$\beta_s=0.01$				$\beta_s=0.1$			
$\beta_t$	0.01	0.1	1	10	0.01	0.1	1	10
Acc	85.4	<b>85.8</b>	85.6	81.1	<u>85.7</u>	<u>85.7</u>	85.4	81.0
	$\beta_s=1$				$\beta_s=10$			
$\beta_t$	0.01	0.1	1	10	0.01	0.1	1	10
Acc	85.4	85.3	85.2	81.2	80.7	80.8	80.5	79.7

Table 11: Ablation on the weight of the final augmented image features.

Compared to zero-shot CLIP, although the text features of MaPLE become more indiscriminable, the image features become more compact and discriminable, presenting a distance trade-off trait between text and image features. It is im-

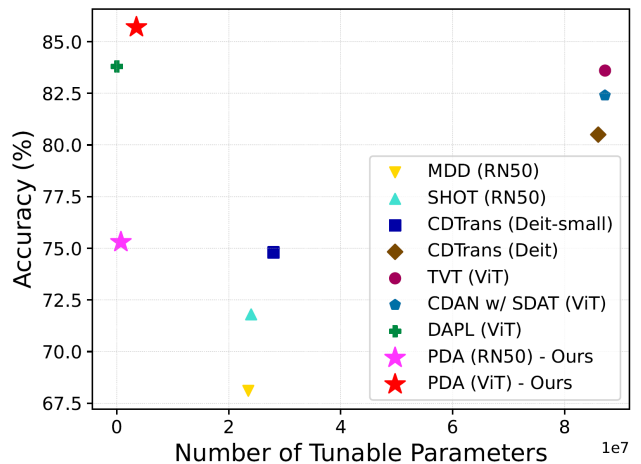


Figure 5: Performance comparison on Office-Home dataset. With much fewer parameters, our PDA method outperforms all other UDA methods

portant to note that MaPLE minimizes the distribution shift due to the lower maximum mean discrepancy (MMD) and KL divergence. Our PDA method further introduces distribution into the prompt, and achieves a lower MMD and KL divergence, indicating the domain discrepancy minimizes. Moreover, we observe that PDA not only achieves a higher inter-class  $L_2$  distance of text features but also a higher  $r$  of image features, indicating both text features and image features become more discriminable.

#### C.4 Ablation Study

**Sensitivity analysis of the weight of the final augmented image features.** As shown in Table 11, we observe that optimal results are achieved when  $\beta_t$  is approximately 0.1 and  $\beta_s$  is around 0.1. However, if the weights of the final augmented image feature become excessively large, it could potentially compromise the model’s discriminative ability.

## C.5 Visualization

**Parameters analysis.** As shown in Figure 5, our PDA method achieves superior results with considerably fewer parameters for both the ResNet50-based model and the ViT-based model.

**Attention.** In Figure 6, we visualize attention maps for different methods. We observe that the visual features of our method get more intensive and prominent.

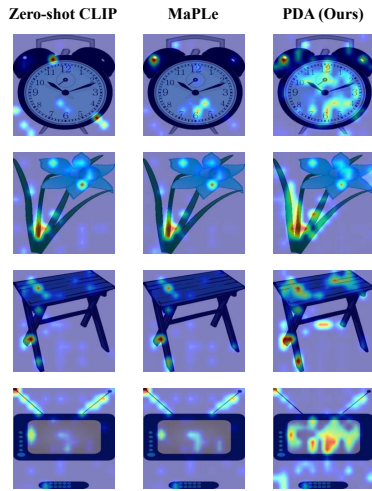


Figure 6: Attention visualization of zero-shot CLIP, MaPLe and PDA methods.